Journal of Physics:
Conference Series

PAPER • **OPEN ACCESS**

Modelling of strain effects in core/shell QDs with tight binding theory and *k.p* effective mass approximation

To cite this article: D Malkoç *et al* 2025 *J. Phys.: Conf. Ser.* **3027** 012044

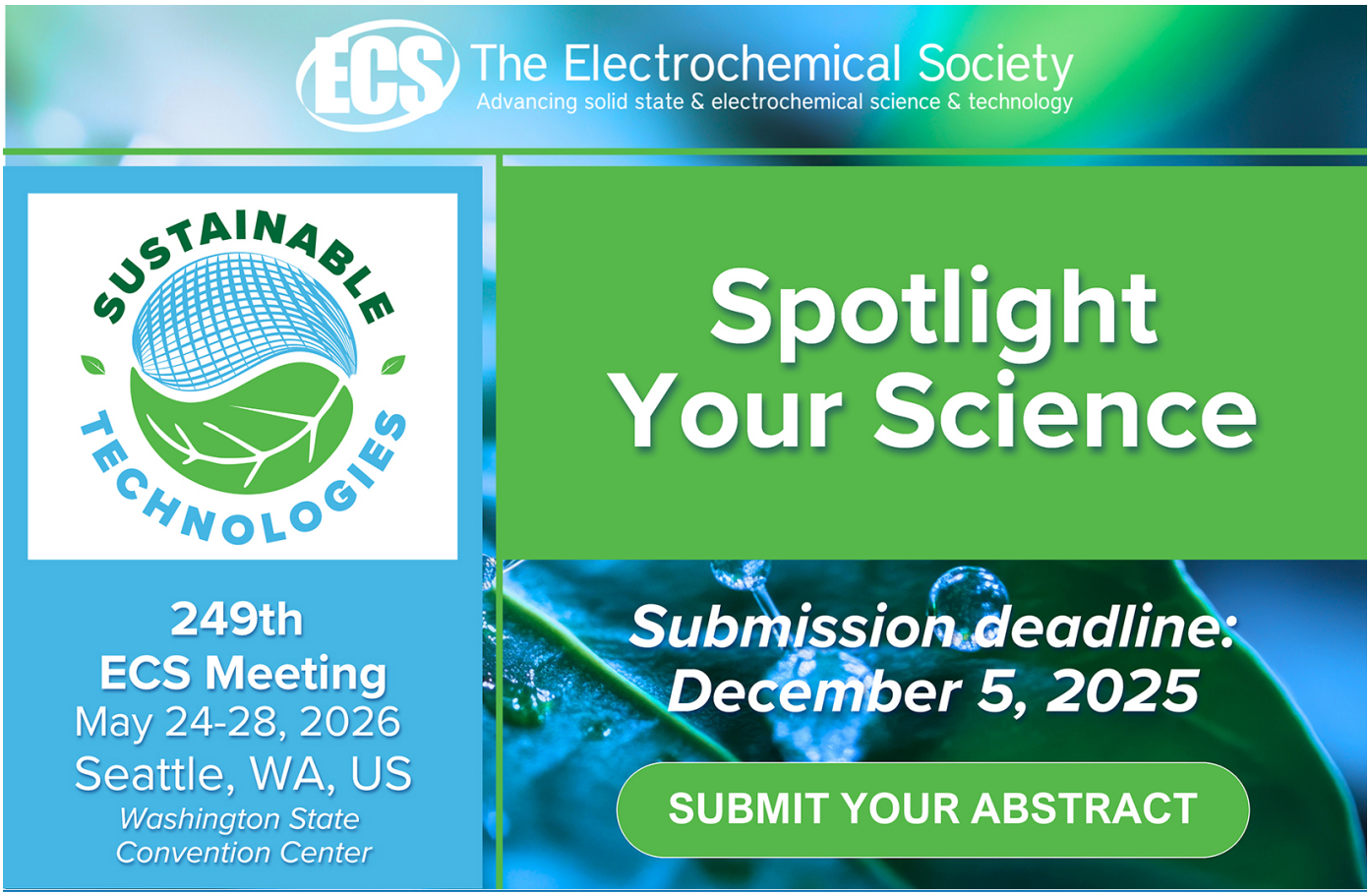

Journal of Physics: Conference Series **3027** (2025) 012044 doi:10.1088/1742-6596/3027/1/012044

Modelling of strain effects in core/shell QDs with tight binding theory and *k.p* effective mass approximation

D Malkoç[1*,2], B Danacı[3] and H Ünlü[1,2]

[1]İstanbul Technical University, Nanoscience and Nanoengineering Programme, Maslak, İstanbul, 34469, Turkey

[2]Fatih Sultan Mehmet Waqf University, Faculty of Engineering, Department of Electrical and Electronics Engineering, Topkapı Campus, İstanbul, 34015, Turkey

[3]Fatih Sultan Mehmet Waqf University, Faculty of Engineering, Department of Software Engineering, Topkapı Campus, İstanbul, 34015, Turkey

*Corresponding author e-mail – malkocd@itu.edu.tr

Abstract. Reliable predictions of the potential of nanoscale semiconductor heterostructures for nanodevice fabrication require accurate theoretical models and precise numerical calculations to assess how strain affects their electronic, optical and structural properties. The second nearest neighbour (2NN) sp3s* tight binding model and the four-band k.p effective mass approximation are employed to analyze impact of strain on the optical, electronic and structural properties in nanoscale spherical CdSe and ZnSe-based core/shell quantum dots (QDs) in this study. According to our analysis, when the shell diameter increases linearly, keeping the core diameter constant, core bandgaps increase parabolically in ZnSe/ZnS and CdSe/Cd(Zn)S QDs but decrease parabolically in ZnSe/CdS QDs. Furthermore, with a constant shell diameter, an increase in core diameter results in a parabolic decrease of core bandgaps in all four QD types. The proposed model can serve as an effective design tool for simulating nanoscale core/shell heterostructures in quantum dot-based nanodevices.

Keywords: CdSe and ZnSe core/shell QDs, Interface strain, Second nearest neighbour (2NN) *sp3s** tight binding theory, k.p effective mass approximations.

1. Introduction

Current growth technologies make it possible to grow core/shell semiconductor heterostructures with groups III-V, II-VI compounds and group IV elemental. Such quantum dots (QDs) can be grown directly on cost-effective substrates like silicon, rather than on more expensive lattice-matched III-V substrates like GaAs. The combination of these features, including light trapping and quantum confinement, makes semiconductor heterostructure core/shell QDs highly attractive for advanced electronic and optical devices, enhancing both performance and functionality.

Colloidal chemical technique enables the production of group II-VI semiconductor nanocrystals (NCs) like CdSe/Cd(Zn)S and ZnSe/Zn(Cd)S, allowing multiple semiconductors to be combined into core/shell heterostructures. These structures are often used to modify the electronic properties of QDs, which can be in the form of Type-I and Type-II configurations [1]. The band offsets in the heterointerface confine holes and electrons within the core region for Type-I heterostructures. However, Type-II heterostructures have a staggered band alignment that spatially separates excited holes and electrons, localizing in either the shell or the core.

The direct transitions of exciton pairs within the core region give rise to the exciton energy for Type I CdSe/Cd(Zn)S QDs, and $E_g^{nc}(d) = hc / \lambda_{\max}$ gives exciton energy of the core. Here, h is the Planck's constant. The speed of light is given by c. The wavelength at which the nanoparticle absorption is maximum is represented by $\lambda_{\max}$. For Type II structures like ZnSe/CdS, the hole is confined to the core, while the electron is confined to the shell, causing an indirect transition from the

conduction band minimum of the shell to the valence band maximum of the core. Bandgaps calculated by using the two-band parabolic effective mass approximation for core/shell QDs are given as [2]

$$E_g^{nc} = E_g^b + \frac{2\hbar^2\pi^2}{m_{cv}^* d^2} - \frac{3.572e^2}{\varepsilon_\infty d} - \frac{0.124e^4}{\hbar^2 m_{cv}^* \varepsilon_\infty^2} \quad (1)$$

Here, E_g^b is the bulk direct bandgap. The kinetic energy for electron-hole pair is given by the second term. The third and last terms represent the Coulomb interaction and the electron-hole correlation energy, respectively. The reduced effective mass for electron-hole pair is given by $m_{cv}^* = (m_e^* m_h^*)/(m_e^* + m_h^*)$ where m_e^* and m_h^* are the effective masses of free electrons and free holes, respectively. ε_∞ represents the optical dielectric constant for bulk semiconductors. Since strain in the interface affects the optical and electronic properties of QDs, one must modify Eq. (1). Thus, a comprehensive computing of band structure in relation to interface strain is crucial to simulate charge transport in nanoscale devices.

We combine the continuum thermoelastic theory [3] with the semi-empirical second nearest neighbour (2NN) sp3s* tight binding (TB) theory and classical *k.p* effective mass approximation to compute the impact of interface strain on the band structure of CdSe/Cd(Zn)S and ZnSe/Zn(Cd)S QDs synthesized by colloidal technique in this work.

2. Calculation methods

Accurate theoretical modelling and precise numerical analysis of interface strain effects on the electronic and optical properties of core/shell QDs are essential for predicting their potential in the fabrication of nanodevices. There are four approaches to obtain the electronic band structure of nanoscale semiconductor devices, which are first-principles ab-initio methods (density functional theory) [4], empirical approaches (local/nonlocal empirical pseudopotential method) [5], TB method [6, 7, 8], and the *k·p* effective mass approximation [9].

2.1 k·p effective mass approximation

The parabolic two-band k·p approximation [8,9] is particularly useful for gaining qualitative insights into the strain effect in QDs and nanowires. In this theory, the electronic states are expressed as a finite linear combination of Bloch states near a band structure extremum within the Brillouin zone, accounting for the spin-orbit interaction. Various theoretical models have been developed since the introduction of the two-band effective mass approximation [2] for calculating core bandgap in spherical core/shell nanostructures. These theories are built upon the four-band model by incorporating spin-orbit coupling as a perturbation, along with the k·p term [9]. This approach aims to minimize the number of parameters by employing the following Hamiltonian [9]

$$H = \frac{p^2}{2m_0} + V(r) + \frac{\hbar^2 k^2}{2m_0} + \frac{\hbar k \cdot p}{m_0} + \frac{\hbar}{4m_0 c^2}(\sigma \times \nabla V) \cdot (\hbar k + p)\,. \quad (2)$$

Matrix elements with eigenfunctions $u_{n,0\uparrow}$ and $u_{n,0\downarrow}$ are generated from $H_{mn} \equiv \langle u_{m,0} \mid H \mid u_{n,0} \rangle$, using the Schrödinger equation within the frame of multiband *k.p* approximation. The details of the solution can be found in literature [10] and will not be repeated here. Near the high symmetry points in the first Brillouin zone, conduction and valence band energy levels are expressed as [11]

$$E_c(k) = -\frac{E_g}{2} + \frac{\hbar^2 k^2}{2m_0} + \frac{E_g}{2}\left(1 + \frac{\hbar^2 k^2 (E_g + \Delta)}{2m_{cv}^* E_g (E_g + 2\Delta/3)}\right)^{1/2} \quad (3)$$

$$E_v(k) = -\frac{E_g}{2} + \frac{\hbar^2 k^2}{2m_0} - \frac{E_g}{2}\left(1 + \frac{\hbar^2 k^2 (E_g + \Delta)}{2m_{cv}^* E_g (E_g + 2\Delta/3)}\right)^{1/2}. \quad (4)$$

Here, the unperturbed band gap is given by $E_g = E_c(0) - E_v(0)$. The dispersion relation ($|k| = \frac{2\pi}{d}$) is due to the quantum size effect of the core with the diameter, d. The spin-orbit interaction is

represented by Δ. We expand the square root terms in Equations (3) and (4) using the Binomial approximation. Hence, the core bandgap becomes

$$E_g^{nc} = E_g^{bi}(\varepsilon_i) + \frac{2\pi^2\hbar^2}{m_{cv}^* d^2}\delta_{sp}\left(1 - \frac{2\pi^2\hbar^2}{m_{cv}^* d^2}\delta_{sp}\right), \quad (5)$$

where the correction factor, $\delta_{sp} = \left(E_g^{bi}(\varepsilon_i) + \Delta_i\right)/\left(E_g^{bi}(\varepsilon_i) + 2\Delta_i/3\right)$ accounts for the spin-orbit interaction's influence on quantum confinement and $E_g^{bi}(\varepsilon_i)$ represents the strain-dependent bulk bandgap. By including the Coulomb interaction and Rydberg correlation energies in Eq. (1), the core bandgap of both bare core and core/shell QDs with Type I band alignment can be derived as follows

$$E_g^{nc}(\varepsilon_i) = E_g^{bi}(\varepsilon_i) + \frac{2\pi^2\hbar^2}{m_{cv}^* d^2}\delta_{sp}\left(1 - \frac{2\pi^2\hbar^2}{m_{cv}^* d^2}\delta_{sp}\right) - \frac{3.572e^2}{\varepsilon_\infty d} - \frac{0.124e^4}{\hbar^2 m_{cv}^* \varepsilon_\infty^2}. \quad (6)$$

For *Type II* band alignment, the core bandgap of heterostructure core/shell QD can be expressed as

$$E_g^{ni}(\varepsilon_i) = E_g^{bi}(\varepsilon_i) - \Delta E_v(\varepsilon_i) + \frac{2\hbar^2\pi^2}{m_{cv}^* d^2}\delta_{sp}\left(1 - \frac{2\pi^2\hbar^2}{m_{cv}^* d^2}\delta_{sp}\right) - \frac{3.572e^2}{\varepsilon_\infty d} - \frac{0.124e^4}{\hbar^2 m_{cv}^* \varepsilon_\infty^2}, \quad (7)$$

where $E_g^{bi}(\varepsilon_i) = E_g^{bi} + \delta E_g^{bi}(\varepsilon_i)$ is the strain-dependent core bandgap with the strain shift, $\delta E_g^{bi}(\varepsilon_i)$, relative to its bulk value, E_g^{bi}, at T=0 K and $\Delta E_v(\varepsilon_i)$ is the valence band offset.

2.2 2NN sp3s TB model*

The semi-empirical 2NN *sp3s** TB model assumes each valence electron is bound to its nuclei tightly, as in a free atom. When anions and cations are sufficiently close so that their separation is on the scale of the semiconductor's lattice constant, their wave functions begin to overlap. According to the Slater-Koster type tight binding formalism [12], the energy levels are determined by finding the eigenvalues of the following matrix

$$\sum_\beta \left[H_{\alpha\beta}(k) - S_{\alpha\beta}(k)E\right]u_\beta = 0. \quad (8)$$

Here, β and α represent the anion s (p) orbital and cation s (p) orbital, respectively. The wave function coefficient is u_β. Since the Bloch functions are orthogonal, the overlap matrix $S_{\alpha\beta} = \langle\varphi_\alpha(k)|\varphi_\beta(k)\rangle$ becomes an identity matrix. $H_{\alpha\beta} = \langle\phi_\alpha(k)|H|\phi_\beta(k)\rangle$ is the (2x2) Hamiltonian matrix with the eigenvalue, E. The on-site and off-site energies $E_{sa}, E_{sc}, E_{pa}, E_{pc}$ and $E_{ss}, E_{xx}, E_{s_a p_c}, E_{s_c p_a}, E_{xy}$ significantly influence the electronic band structure characteristics. The off-site TB matrix elements are adjusted by the interface strain. These elements are determined by the Harrison Scaling rule [12] $V_{ll'm}(\varepsilon) = V_{ll'm}(a/a_o)^{-\eta_{llm}}$. Here, the interaction potential (for anion and cation atoms), $V_{ll'm}(\varepsilon)$ and $V_{ll'm}$, correspond to the strained and bulk values, respectively. To model the strain-dependent band structure, η_{llm} are obtained using the volume deformation potential, $a_{gl} = -B(\partial E_{gl}/\partial P)$ of $E_{g\Gamma}, E_{gL}$ and E_{gX} band gaps at symmetry points under hydrostatic pressure.

3. Results and Discussion

3.1Band structure calculations for bulk semiconductors

Material parameters used in computing the electronic band structures for CdSe, ZnSe, CdS, and ZnS semiconductors by using the semi-empirical 2NN sp^3s^* TB theory and 4-band k·p effective mass approximation are listed in Tables 1 and 2, respectively. Furthermore, in Table 3, the common parameters for optimizing the TB parameters and k.p parameters are shown.

Table 1. TB parameters used in computing the band structures which are obtained by 2NN sp^3s^* TB theory for CdSe, ZnSe, CdS and ZnS bulk semiconductors [8].

Parameters	CdSe	ZnSe	CdS	ZnS
$E_{s,a}$ (eV)	-9.63	-11.97	-11.53	-11.61
$E_{p,a}$ (eV)	1.326	1.51	0.53	1.48
$E_{s,c}$ (eV)	0.03	1.29	1.83	1.11
$E_{p,c}$ (eV)	4.73	5.99	5.87	6.52
$E_{s^*,a}$ (eV)	7.53	11.58	7.13	8.08
$E_{s^*,c}$ (eV)	5.72	8.72	6.87	8.02
$4V_{s,s}$ (eV)	-4.64	-5.0	-3.07	-6.30
$4V_{x,x}$ (eV)	2.64	3.0	1.76	3.11
$4V_{x,y}$ (eV)	5.36	5.99	4.23	5.00
$4V_{s,p}$ (eV)	4.57	5.97	2.17	5.16
$4V_{p,s}$ (eV)	5.54	4.49	5.48	5.17
$4V_{s^*,p}$ (eV)	3.05	5.64	1.99	2.89
$4V_{p,s^*}$ (eV)	2.49	3.19	3.06	1.75
ε_{sx} (eV)	0.0	-0.15	0.10	0.20
ε_{xy} (eV)	0.0	0.60	-0.01	-0.15
λ_a (eV)	0.14	0.16	0.03	0.03
λ_c (eV)	0.06	0.03	0.01	0.03

Table 2. Parameters used in computing the band structure which are obtained by k.p effective mass approximation for bulk semiconductors

Parameters	CdSe	ZnSe	CdS	ZnS
E_g (0) (eV)	1.823	2.823	2.552	3.820
$-E_v$ (eV)	11.49	12.65	12.61	14.66
a_g (eV)	-2.9[a]	-5.82[b]	-2.94[a]	-6.4[b]
a_v (eV)	0.9[a]	1.65[b]	0.40[a]	2.31[b]
γ_1	3.33[c]	3.77[d]	4.11[e]	2.54[d]
γ_2	1.11[c]	1.24[d]	0.77[e]	0.75[d]
γ_3	1.11[c]	1.67[d]	1.53[e]	1.09[d]

[a]Ref. [13]; [b]Ref. [14]; [c]Ref. [15]; [d]Ref. [16]; [e]Ref. [17].

Table 3. Common material parameters used in 2NN sp^3s^* TB theory and k.p approximation [17, 18]

Parameters	CdSe	ZnSe	CdS	ZnS
a (nm)	0.607	0.5668	0.581	0.541
E_g (0) (eV)	1.899	2.824	2.503	3.702

$-E_v$ (eV)	11.50	13.85	12.20	14.20
Δ (eV)	0.410	0.424	0.070	0.092
a_g (eV)	-2.89	-5.1	-2.90	-5.2
a_v (eV)	0.9	1.23	0.40	0.83
$\varepsilon_\infty/\varepsilon_0$	5.80	5.56	5.24	5.20
C_{11} (10^{11} dyn/cm^2)	6.67	8.57	7.70	10.11
C_{12} (10^{11} dyn/cm^2)	4.63	5.07	5.39	6.46
C_{44} (10^{11} dyn/cm^2)	2.23	4.05	2.36	4.46
α_{th}(10^{-6} K^{-1})	7.30	7.60	4.05	6.9
α (10^{-4} eV)	6.96	5.58	3.45	10
β (K)	281	187	208	600

The band structures of CdSe, ZnSe bulk semiconductors calculated by using the two models are shown in Figure 1. As can be seen from Table 2 and Table 3, bandgaps calculated by using both models are in excellent agreement.

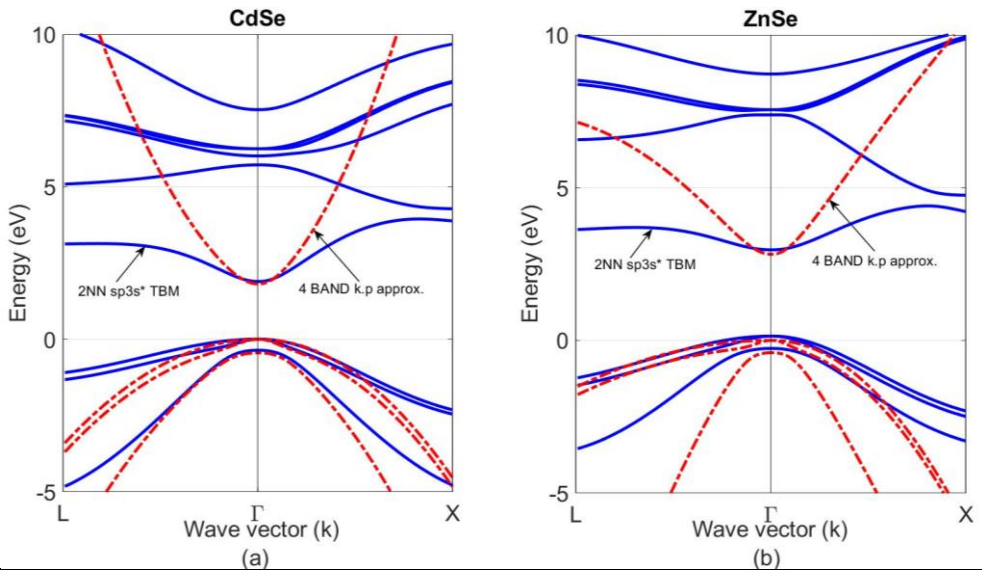

Figure 1. Comparison of the band structure of (a) CdSe and (b) ZnSe bulk semiconductors due to *2NN* sp^3s^* TB model and 4 band *k.p* effective mass approximation.

Notably, bulk model calculations overlook the impact of core and shell dimensions, the differences in elastic constants and linear thermal expansion coefficients, as well as the spin-orbit splitting effect on the constituents when computing interface strain in QDs.

3.2 Strain effect on core bandgap of core/shell QDs

Classical continuum elasticity theories do not adequately account for factors such as alloy composition, dimensions, differences in the elastic constants, the free thermal expansion of lattice constants and linear thermal expansion coefficients. Group IV elemental semiconductors, as well as II-VI, III-V compound semiconductors, are known to undergo expansion with increasing temperature during

crystal growth, preserving their crystal structure [19]. Hence, it is essential to account for the thermal strain and the lattice thermal expansion effects due to localized mechanical stress while the crystal grows in the heterointerface.

During core/shell QD formation, a potential step appears in the valence band whereas a potential barrier occurs in the conduction band at the interface. According to continuum elasticity theory [19, 20], the uniaxial component of the biaxial strain tensor results in the splitting of the heavy-hole, light-hole, and split-off valence band edges in relation to the average valence band edge. Additionally, the hydrostatic component of the biaxial strain tensor induces a shift in both the conduction and valence band edges compared to their unstrained values.

We use the continuum elastic model to illustrate the strain effect in spherical core/shell QDs [3]. The equilibrium equation in Hooke's law is written as [19, 20]

$$\frac{d\sigma_r}{dr} + \frac{2}{r}(\sigma_r - \sigma_t) = 0, \tag{9}$$

which is solved by using boundary conditions such as continuity of stress, $\sigma_{ir}(a) = \sigma_{mr}(a) = -P_i$, lattice mismatch discontinuity of tangential strain at the interface and absence of stress in the region outside the core/shell structure ($\sigma_{mr}(b) = P_o = 0$). *Shrink fit condition* [19, 20] becomes

$$|r(\varepsilon_{m\theta} - \varepsilon_{i\theta})|_{r=a} = a\varepsilon_{im} = \frac{a(a_i - a_m)}{a_m}. \tag{10}$$

Here, *a* is the core radius. In the core region, the stress is obtained as $\sigma_{ir} = \sigma_{i\theta} = \sigma_{i\varphi} = \sigma_i = -P_i$. The radial and tangential strains in the interface are found in the core region as follows [3]

$$\varepsilon_i = \frac{(1-2\nu_i)\sigma_i}{E_i} + \alpha_i T = -\frac{(1-2\nu_i)P_i}{E_i} + \alpha_i T. \tag{11}$$

The radial and tangential strains for the shell region are obtained as [3]

$$\varepsilon_{mr} = \frac{P_i\left((1-2\nu_m)a^3 - (1+\nu_m)b^3\right)}{E_m(b^3 - a^3)} + \alpha_m T \tag{12a}$$

$$\varepsilon_{mt} = \frac{P_i\left((1-2\nu_m)a^3 - (1+\nu_m)b^3\right)}{E_m(b^3 - a^3)} + \alpha_m T. \tag{12b}$$

Combining Eqs. (12a) and (12b) with Equation (11), contact pressure at the interface becomes [3]

$$P_i = \frac{2E_iE_m[1-(a/b)^3][\varepsilon_{im} + (\alpha_i - \alpha_m)T]}{C + 2D(a/b)^3}, \tag{13}$$

where constants C and D are given as $C = [(1+\nu_m)E_i + 2(1-2\nu_i)E_m]$ and $D = [(1-2\nu_m)E_i - (1-2\nu_i)E_m]$. On substitution of Eq. (13) into Eq. (11), the strain is found on the core region. Substitution of Eq. (13) into Equations (12a) and (12b), one finds the strain on the shell region. The bandgap depending on temperature and pressure is given as [21]

$$E_{gi}(T,P) = E_{gi} + \Delta C_{iP}^0 T(1 - ln\,T) - \frac{a_{gi}}{B}\left(1 - \frac{P_i}{2B} - \frac{(1+B')P_i^2}{3B^2}\right)P_i. \tag{14}$$

Here, the bulk bandgap for 0 K is denoted by E_{gi}, the second term gives the contribution of the lattice vibration, and the core/shell interface strain effect is given by the last term, respectively. B is the bulk modulus and $B' = \partial B/\partial P$. The standard state heat capacity for electron-hole pair formation, ΔC_{iP}^0, is found by fitting Equation (14) to the experimental values of the bandgap for bulk at constant pressure and any given temperature.

The impact of core and shell diameter on the core bandgap of the four QDs at 300 K is shown in Figure 2 and Figure 3. They are calculated by using *2NN sp3s** TB model and 4-band *k.p* approximation. Comparison of Figures 2 and 3 indicate that both *2NN sp3s** TB model and 4-band *k.p* approximation predict a parabolic decrease in the core bandgap of the four QDs when the core diameter increases linearly, keeping the shell diameter constant. Figures 2 and 3 indicate that both *2NN sp3s**

TB model and 4-band *k.p* approximation predict a parabolic increase in the core band gap for CdSe/Cd(Zn)S and ZnSe/ZnS QDs when the shell diameter increases linearly, keeping the core diameter constant. Both theories predict a parabolic decrease of the core bandgap in ZnSe/CdS QDs due to changes in the sign of thermoelastic hydrostatic strain across the ZnSe/CdS heterointerface. The results show that the two theories are compatible with each other.

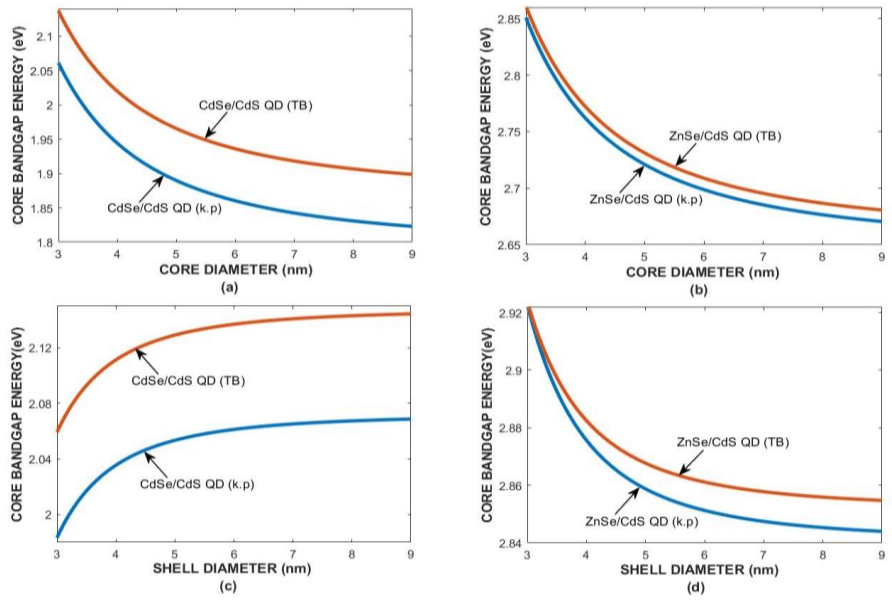

Figure 2. Comparison of the 2NN sp3s* TB theory and 4-band k·p effective mass approximation showing the effects of (a, b) core diameter and (c, d) shell diameter on the core bandgaps for CdSe/CdS (left) and ZnSe/CdS (right) QDs.

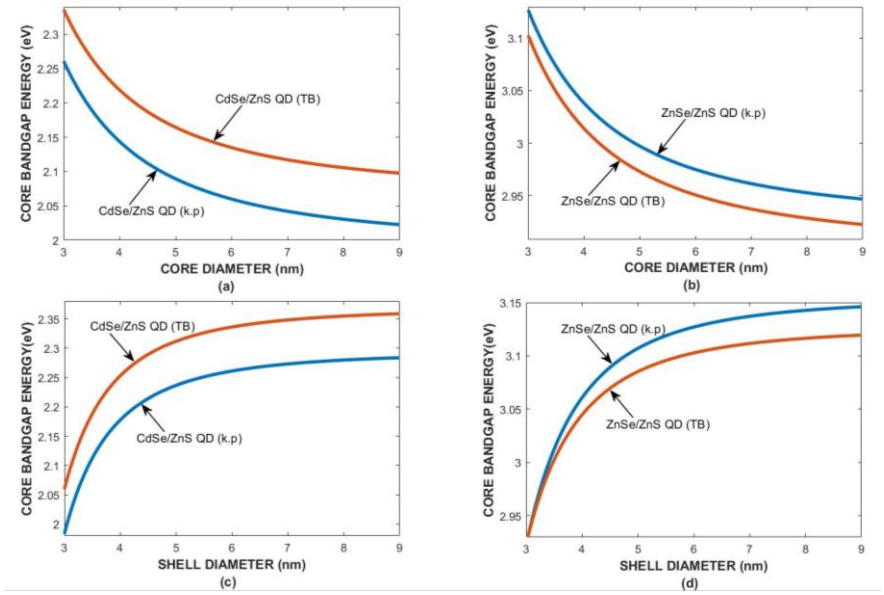

Figure 3. Comparison of the 2NN sp3s* TB theory and 4-band k·p effective mass approximation showing the effects of (a, b) core diameter and (c, d) shell diameter on the core bandgaps for CdSe/ZnS (left) and ZnSe/ZnS (right) QDs.

4. Conclusions

The impact of strain on the core bandgaps in CdSe/Cd(Zn)S and ZnSe/Zn(Cd)S QDs was investigated by using 2NN *sp3s** TB model and four-band *k·p* effective mass approximation. Calculations show that core bandgaps decrease parabolically when the core diameter increases linearly, keeping the shell diameter constant and that core bandgaps increase parabolically when the shell diameter increases linearly, keeping the core diameter constant in CdSe/Cd(Zn)S and ZnSe/ZnS QDs. However, both theories predict a parabolic decrease of the core bandgaps in ZnSe/CdS QDs due to changes in the sign of thermoelastic hydrostatic strain across the ZnSe/CdS heterointerface. The results suggest that the proposed model can serve as an effective design tool for simulating nanoscale core/shell heterostructures in quantum dot-based nanodevices.

Acknowledgments

One of us (H. Ünlü) is supported by Fatih Sultan Mehmet Waqf University Research Foundation (Project No: 2023B1Ç08D).

References

[1] H. Ünlü and N. M. Horing (Editors), Progress in Nanoscale and Low-Dimensional Materials and Devices: Properties, Synthesis, Characterization, Modelling and Applications
[2] L. E. Brus, J. Chem. Phys. 80, 4403 (1984).
[3] H. Ünlü, The European Physical Journal Applied Physics, 86 (3), 30401 (2019).
[4] P. Hohenberg and W. Kohn, Phys. Rev. 136 B, 864 (1964).
[5] M.L. Cohen and J. R. Chelikowsky, Electronic Structure and Optical Properties of Semiconductors (2nd Ed.), Springer-Verlag (1989).
[6] Ö . Akıncı, Ö., H.H. Gürel, H.H. and H. Ünlü, Thin Solid Films, 517, 2431 (2009).
[7] H. H. Gürel, Ö. Akıncı, H. Ünlü, Computational Material Science, 33, 269 (2005).
[8] H. Gürel and H. Ünlü, Materials Science in Semiconductor Processing, 36, 1619 (2013).
[9] E. O. Kane. J. Phys. Chem. Solids 1, 249 (1957).
[10] M. Ehrhardt and T. Koprucki (Eds.), Multi-band effective mass approximations, Springer (2014).
[11] H. E. Ghassan, Al-Shabeeba, and A.K. Arof, Eur. Phys. J. Plus, 128, 153 (2013).
[12] W. A. Harrison, Electronic Structure and the Properties of Solids, Freeman (1980).
[13] Li YH, Gong XG, Wei SH. Ab initio all-electron calculation of absolute volume deformation potentials of IV–IV, III–V, and II–VI semiconductors: the chemical trends. Physical Review B. 2006;73:245206(1–5).
[14] Van de Walle CG. Band lineups and deformation potentials in the model-solid theory. Physical Review B. 1989;39(3):1871.
[15] Mourad D, Richters JP, Gerard L, Andre R, Bleuse J, Mariette H. Determination of the valence band offset at cubic CdSe/ZnTe type II heterojunctions: a combined experimental and theoretical approach.
[16] Lawaetz P. Valence-band parameters in cubic semiconductors. Physical Review B.1971;4(19):3460–3467.
[17] Sadao Adachi, Wiley Series in Materials for Electronic and Optoelectronic Applications, John Wiley & Sons Ltd, (2005).
[18] O. Madelung, in Numerical Data and Functional Relationships in Science and Technology (Springer, Berlin, 1984), Part d of Vol. 17
[19] J. R. Barber, Elasticity, 3rd Ed. (Springer, Dordrecht Heidelberg London New York, 2010).
[20] A. S. Saada, Elasticity Theory and Applications, Pergamon, New York, (1974).
[21] H. Ünlü, Solid State Elect. 35 (1992) 1343.